J Comput Aided Mol Des (2012) 26:963–976
DOI 10.1007/s10822-012-9588-4

Combining conformational sampling and selection to identify the binding mode of zinc-bound amyloid peptides with bifunctional molecules

Liang Xu · Ke Gao · Chunyu Bao · Xicheng Wang

Received: 31 March 2012 / Accepted: 5 July 2012 / Published online: 25 July 2012

Abstract The pathogenesis of Alzheimer's disease (AD) has been suggested to be related with the aggregation of amyloid β (Aβ) peptides. Metal ions (e.g. Cu, Fe, and Zn) are supposed to induce the aggregation of Aβ. Recent development of bifunctional molecules that are capable of interacting with Aβ and chelating biometal ions provides promising therapeutics to AD. However, the molecular mechanism for how Aβ, metal ions, and bifunctional molecules interact with each other is still elusive. In this study, the binding mode of Zn^{2+}-bound Aβ with bifunctional molecules was investigated by the combination of conformational sampling of full-length Aβ peptides using replica exchange molecular dynamics simulations (REMD) and conformational selection using molecular docking and classical MD simulations. We demonstrate that Zn^{2+}-bound $A\beta_{(1–40)}$ and $A\beta_{(1–42)}$ exhibit different conformational ensemble. Both Aβ peptides can adopt various conformations to recognize typical bifunctional molecules with different binding affinities. The bifunctional molecules exhibit their dual functions by first preferentially interfering with hydrophobic residues 17–21 and/or 30–35 of Zn^{2+}-bound Aβ. Additional interactions with residues surrounding Zn^{2+} could possibly disrupt interactions between Zn^{2+} and Aβ, which then facilitate these small molecules to chelate Zn^{2+}. The binding free energy calculations further demonstrate that the association of Aβ with bifunctional molecules is driven by enthalpy. Our results provide a feasible approach to understand the recognition mechanism of disordered proteins with small molecules, which could be helpful to the design of novel AD drugs.

Keywords Replica exchange molecular dynamics simulations · Amyloid · Alzheimer's disease · Bifunctional molecules · Metal ions

Abbreviations

AD	Alzheimer's disease
Aβ	Amyloid-β
REMD	Replica exchange molecular dynamics
HBX	2-(2-Hydroxylphenyl)benzoxazole
MPY′	4-(5-Hydoxylimidazo[1,2-a]pyridin-2-yl)-N,N-dimethylaniline
L2B	N1,N1-dimethyl-N4-(pyridin-2-ylmethyl)benzene-1,4-diamine
EDTA	Ethylenediaminetetraacetic acid
CQ	Clioquinol, 5-chloro-7-iodo-8-hydroxyquinoline
PBT2	8-Hydroxyquinoline derivative

Introduction

Accumulated evidence has suggested that the pathology of Alzheimer's disease (AD) is associated with amyloid β (Aβ) peptides (amyloid hypothesis) [1–3]. Conformational transitions from soluble disordered Aβ monomers into insoluble, highly ordered fibrils through more toxic oligomers have been proposed to be crucial steps in the

Electronic supplementary material The online version of this article (doi:10.1007/s10822-012-9588-4) contains supplementary material, which is available to authorized users.

L. Xu (✉) · K. Gao · C. Bao
School of Chemistry, Dalian University of Technology, Dalian 116024, China
e-mail: xuliang@dlut.edu.cn

X. Wang
Department of Engineering Mechanics, State Key Laboratory of Structural Analyses for Industrial Equipment, Dalian University of Technology, Dalian 116023, China

development of AD [4]. Moreover, metal ions, especially Zn, Cu, and Fe, have also been implicated to participate in the process of Aβ aggregation and production of reactive oxygen species initiated by Aβ peptides (metal hypothesis) [5–9].

Aβ peptides are produced from the amyloid precursor protein (APP), containing 39–43 amino acids. A$\beta_{(1-40)}$ has been found as the most abundant form whereas A$\beta_{(1-42)}$ is believed to be more toxic [10]. Transition metal ions such as zinc and copper can interact with Aβ primarily via binding to the hydrophilic N-terminal region (i.e., residue 1–16) [11–14]. Recent advancements in experimental studies have implicated that the possible binding sites for Cu ions involve Asp^1, Ala^2, His^6, His^{13}, and His^{14} of Aβ. In addition, Glu^3, Asp^7, and Glu^{11} are also suggested as the coordination sites for Cu [14–16]. The binding sites for Zn^{2+} include Asp^1, Glu^{11}, His^6, His^{13}, and His^{14} [14–18]. Recent nuclear magnetic resonance (NMR) experimental studies on the interactions of Zn^{2+} with termini-blocked A$\beta_{(1-16)}$ peptide confirmed that His^6, Glu^{11}, His^{13}, and His^{14} are the minimal Zn^{2+} binding sites of Aβ peptides [19, 20]. Assuming that A$\beta_{(1-16)}$/A$\beta_{(1-28)}$ and A$\beta_{(1-40)}$/A$\beta_{(1-42)}$ share the same coordination sites, both A$\beta_{(1-16)}$ and A$\beta_{(1-28)}$ have been widely used to investigate the coordination chemistry of full-length Aβ peptides [12, 19, 21–30]. Although the exact metal binding sites are still controversial for Aβ, polymorphism, which has been recognized recently to understand the polymorphic states of Aβ conformations [10], Aβ oligomers [31–33], and Aβ aggregation induced by metal ions such as Zn^{2+} [34], Cu^{2+}[35], and possibly Al^{3+} [36], seems to be a general property of amyloidogenic proteins [37].

Based on amyloid hypothesis, different kinds of amyloid inhibitors (for example, small molecules [38–43], short peptides [44, 45], and nanoparticles [46]) have been developed to disassemble amyloid aggregation. Meanwhile, traditional metal chelating agents, such as EDTA, CQ, PBT2, and cyclen, have already been utilized as therapeutic agents to disrupt the metal and Aβ interactions [47–51]. Some molecules like CQ and PBT2 have been shown to improve the cognition behavior by reducing the amount of plaque deposits in phase II clinical trials. However, the adverse side effects limit their long-term use [47, 48]. In addition, it has been demonstrated that CQ could not completely inhibit Aβ aggregation [52]. The introduction of metal hypothesis into amyloid hypothesis has led to a novel potential therapeutic way to treat AD by creating diverse bifunctional molecules that are able to interact with Aβ and chelate metal ions as well. For example, Some small molecules that contain structural motifs for Aβ recognition and metal chelation has been designed and tested experimentally (in vitro) [53–55]. The addition of metal binding agents to short peptide A$\beta_{(16-20)}$ generates another kind of bifunctional molecules [56, 57]. Here, we focus on three bifunctional small molecules as shown in Fig. 1. Understanding the binding mode of Aβ by these small molecules is crucial in the design of new chemical compounds as potential drugs for AD [58]. However, the molecular mechanism of how Aβ interacts with small molecules in the presence or absence of metal ions is still elusive. Due to the dynamic nature and polymorphic states of Aβ, it is rather difficult to capture the binding sites of small compounds through in vitro experiments. Theoretical studies also face great challenges because the time scale required for conformational changes induced by small molecules is still far beyond the accessible computation time in terms of the "induced fit" hypothesis of protein–ligand interactions [59]. An alternative hypothesis termed conformational selection has been emerged based on experimental results, which assumes that the ligand first selects the most favored pre-existing conformations of a protein, and then the binding interactions lead to redistribution of the relative conformations in solution (population shift) [59].

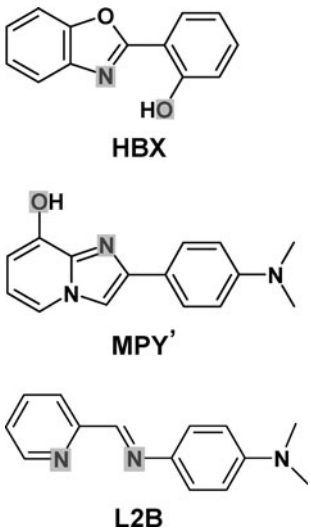

Fig. 1 Chemical structures of bifunctional molecules (HBX, MPY′, and L2B) studied in the present work. The metal binding atoms are highlighted in *grey shading*

Inspired by the conformational selection model, the combination of conformational sampling and selection was applied in this study to investigate the binding mechanism of Zn^{2+}-bound Aβ (Aβ–Zn^{2+}) with bifunctional molecules. Specifically, we focus on the interactions of three bifunctional molecules (as shown in Fig. 1) with full-length Aβ peptides (A$\beta_{(1-40)}$ and A$\beta_{(1-42)}$ monomers) that have Zn^{2+} coordinated to residues His^6, Glu^{11}, His^{13}, and His^{14} of each peptide. In addition to metal binding properties, HBX was found to be a potential biomarker for amyloid aggregation [53], MPY′ has been reported to be able to modulate copper-induced Aβ aggregation [54], and

recent studies showed that L2B was able to disassemble Aβ aggregates induced by copper or zinc ions [55]. The conformational space of Aβ–Zn^{2+} was first sampled by extensive REMD simulations [60, 61]. Then the conformational selection was performed by blindly docking the ligands (shown in Fig. 1) into the clustered conformations of Aβ–Zn^{2+}. The binding affinity was subsequently ranked based on the docking energies [62, 63]. Finally, the ligand–Aβ–Zn^{2+} complexes with high binding affinities were chosen as initial structures and subjected to classical MD simulations. Binding free energy calculations using the molecular mechanics/generalized Born surface area (MM/GBSA) method were carried out to quantitatively evaluate the mode of interactions [64]. Our results clearly show the difference of conformational spaces sampled by Zn^{2+}-bound A$\beta_{(1-40)}$ and A$\beta_{(1-42)}$. There are no dominant binding modes for the association of bifunctional molecules and Aβ–Zn^{2+}. Importantly, we suggest that these small molecules display their dual functions in a consecutive way, i.e., Aβ interaction followed by metal chelation. Moreover, the formation of a stable liang–Aβ–Zn^{2+} complex is an enthalpy-driven process where hydrophobic interactions are crucial for their binding affinity.

Methods

Amber force field parameters for Aβ–Zn^{2+}

The coordinates of model structure used to calculate the Amber force field parameters for Aβ–Zn^{2+} was based on the NMR structure of Zn^{2+}-bound A$\beta_{(1-16)}$ with acetylated N-terminus and amidated C-terminus (PDB ID: 1ZE9) [19, 20]. In this structure, one zinc ion binds per Aβ, resulting in 1:1 Zn^{2+}:Aβ molar ratio. Four residues, i.e., His^{6}, His^{13}, His^{14}, and Glu^{11}, were identified to coordinate with Zn^{2+} through N^{δ}, N^{ε}, N^{δ}, and carboxylate O atoms, respectively. Consistent with previous studies, each His residues was modeled as an imidazole molecule. Residue Glu^{11} was simplified as an acetic acid structure [65–67]. The RESP method was employed to obtain the partial charges [68] (Fig. S1). The bonded and non-bonded parameters were taken from previous studies on the same model structure [67]. The computational details and the force filed parameters were provided in the Supplementary Material. It was found that charge transferred from ligands (His or Glu) to Zn^{2+}, following the classical ligand-to-metal charge transfer (LMCT) mechanism (Table S1). The geometry of the Zn^{2+}-binding site was calculated and compared with NMR experimental data and previous studies (Table S2). A good agreement was achieved (Table S2), indicating that the force field used here was capable of maintaining the metal coordination environment.

Conformational sampling of A$\beta_{(1-40)}$–Zn^{2+} and A$\beta_{(1-42)}$–Zn^{2+} by REMD simulations

The A$\beta_{(1-42)}$–Zn^{2+} structure was constructed by linking the experimental structure of A$\beta_{(1-16)}$–Zn^{2+} (PDB ID: 1ZE9) with one structure of A$\beta_{(17-42)}$ fibrils (PDB ID:2BEG) [69]. Note that such model structure of full-length Aβ–Zn^{2+} has been used to study the conformational difference of Aβ with/without Zn^{2+} [70], and probe the structural populations of Aβ fibrils promoted by zinc ions [34, 71]. REMD simulations have been extensively used as an efficient sampling technique in order to explore the rugged energy landscape of Aβ [70, 72–74]. In REMD simulations, N independent replicas are simulated at N different temperatures in parallel. The exchange among neighboring replicas is attempted at a specific interval with the acceptance ratio determined by the Metropolis criteria:

$$p = \exp\left[-(\beta_j - \beta_i)(E_i - E_j)\right]$$

where $\beta = 1/(k_B T)$ (k_B is the Boltzmann constant and T is the temperature). E_i and E_j are the potential energies at states i and j with corresponding temperatures T_i and T_j, respectively. In the present study, 16 replicas were used for each Aβ–Zn^{2+} simulation with temperatures exponentially distributed between 280 and 408 K (280.0, 287.0, 294.3, 301.7, 309.4, 317.2, 325.2, 333.5, 342.0, 350.7, 359.7, 368.9, 378.3, 388.0, 397.9, and 408.1 K). Note that previous REMD simulations has shown that the final results are independent from the initial conformations of the peptides [75]. The initial conformations of each replica were first minimized and then equilibrated for 200 ps at different temperatures using different random seeds. The time interval of exchange between replicas was set to 5 ps and the final exchange probability was about 52 and 51 % for A$\beta_{(1-40)}$–Zn^{2+} and A$\beta_{(1-42)}$–Zn^{2+} systems, respectively. All REMD simulations were performed using Amber11 [76] with Amber ff99SB force fields [77] and a modified Generalized Born model (Onufriev-Bashford-Case model) [78]. Langevin thermostat was applied to control the temperature of the system. The integration time step was set to 2 fs, and each trajectory was saved every 500 steps (1 ps). The production run for each replica was set to 200 ns, resulting in a total simulation time of 3.2 μs for each system. Only the last 100 ns of each trajectory at physiological temperature of 310 K (corresponding to the replica at 309.4 K) was used for data analysis.

Conformational selection of ligand–Aβ–Zn^{2+} structures by docking

For each REMD simulations, the algorithm described by Daura et.al. [79] was used to cluster the last 100 ns trajectory with a RMSD threshold of 3.0 Å. The central structures

collected from the top 200 clusters were used as the representative conformations for each system. Blind docking studies were conducted using AutoDock4 software [62, 63]. The Lamarckian generic algorithm with a 3D grid box spanning the whole Aβ peptide was applied to search the possible binding sites for each ligand (HBX, MPY′ and L2B). Total 200 conformations of each Aβ–Zn^{2+} were tested for each ligand and the final binding conformations were clustered using the method implemented in AutoDockTools1.5 [62, 63]. The conformations of ligand–Aβ–Zn^{2+} were selected from the top 5 clusters with the higher occurrence and lower binding energies predicted by AutoDock.

Because every conformation of Aβ–Zn^{2+} used in docking only represents the central conformation of that cluster, it is possible that other conformations in the same cluster display higher binding affinity to the ligand. Hence, conformation searching was also performed on those clusters with central structures showing lower binding energies.

MD simulations of the interactions between Aβ–Zn^{2+} and ligands

The starting structures for MD simulations were taken from the above docking studies. The same Amber ff99SB force fields were used to model Aβ structure. The general Amber force fields (GAFF) [80, 81] were applied to HBX, MPY′, and L2B. Each system was solvated in a cubic box filled with TIP3P water molecules [82]. The minimal distance between any atom of ligand–Aβ–Zn^{2+} complex and the box boundary is at least 12 Å. Counter ions were added to neutralize each system. Periodic boundary conditions were applied for three dimensions. The van der Waals (VDW) interactions were calculated with a cutoff of 12 Å, and PME method was used to treat long-rang electrostatic interactions [83]. Langevin dynamics was employed to control the temperature of each system at 310 K. The integration time was 2 ps with bond length involving hydrogen atoms were constrained by LINCS algorithm [84]. Every system was equilibrated by carrying out 10-ps minimization, 50-ps heating and density equilibration with weak constraints on ligand–Aβ–Zn^{2+} structure, and 500-ps constant pressure equilibration at 310 K. The production run of each MD simulation was performed at least 30 ns and the trajectory was save every 1 ps.

MD simulations of the interactions between Zn^{2+} and ligands

In addition to the interactions with Zn^{2+}-bound Aβ peptides, the metal binding properties of HBX, MPY′ and L2B were investigated using MD simulations. The computational details were provided in the Supplementary Material.

Binding free energy calculations by MM/GBSA method

The binding free energy was calculated using the MM/GBSA method [64]:

$$\Delta G = \Delta H - T\Delta S$$
$$\Delta H = \Delta E_{\mathrm{MM}} + \Delta G_{\mathrm{solvation}}$$

where Δ is the difference between the bound and free states of Aβ–Zn^{2+} and ligand. The E_{MM} term is the internal energy (a sum of electrostatic and VDW interaction energies). The solvation free energy includes the electrostatic contribution and the non-polar part that is proportional to the solvent accessible surface area of Aβ–Zn^{2+}. The entropy S was calculated by applying normal mode analysis on trajectories obtained from MD simulations.

Results and discussion

Characterization of the conformational spaces of A$\beta_{(1–40)}$–Zn^{2+} and A$\beta_{(1–42)}$–Zn^{2+}

The convergence of our REMD simulations was first tested by calculating the cumulative average of helix content (α-helix + π-helix + 3_{10}-helix) for each system because previous studies have demonstrated that this value can be used to validate the convergence of REMD simulations [85]. Apparently, as shown in Fig. S2, each REMD simulation was well converged after 100 ns. Consequently, only the last 100-ns trajectory of each system was used for data analysis.

The conformational distributions of A$\beta_{(1–40)}$–Zn^{2+} and A$\beta_{(1–42)}$–Zn^{2+} were first characterized by cluster analysis and results were depicted in Fig. 2. Among the top 200 clusters, there is discernable difference that can be found in the top 15 clusters. In particular, the populations of top 5 clusters in A$\beta_{(1–40)}$–Zn^{2+} system are 11.1, 3.4, 2.8, 2.3, and 1.8 %. The corresponding values are 6.5, 5.3, 5.2, 3.3, and 3.2 % for A$\beta_{(1–42)}$–Zn^{2+} system. Thus, the conformational space of A$\beta_{(1–40)}$–Zn^{2+} is primarily dominated by one cluster (11.1 %), whereas several comparable size of clusters are present in the conformational ensemble of A$\beta_{(1–42)}$–Zn^{2+}. This result suggests that the conformational space of A$\beta_{(1–42)}$–Zn^{2+} is more heterogeneous than that of A$\beta_{(1–40)}$–Zn^{2+}.

Principle component analysis (PCA) was also performed to construct the free energy surfaces of A$\beta_{(1–40)}$–Zn^{2+} and A$\beta_{(1–42)}$–Zn^{2+} in a two-dimensional space (Fig. 3). Both energy landscapes display two common features: a global energy minimum (indicated by cross symbol) in a small region and several local energy minima that are separated by shallow energy barriers. The latter feature is more pronounced for A$\beta_{(1–42)}$–Zn^{2+} system where more conformational basins

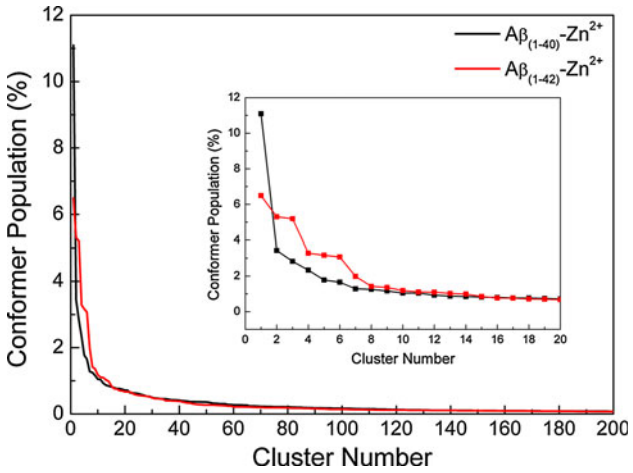

Fig. 2 Cluster populations of the 200-ns REMD simulations of A$\beta_{(1–40)}$–Zn^{2+} and A$\beta_{(1–42)}$–Zn^{2+} system (1:1 Zn^{2+}:Aβ molar ratio). Inset shows the top 20 cluster populations of these two systems

were identified and separated by the barriers (<2.0 kcal/mol). As a result, the free energy surface of A$\beta_{(1–42)}$–Zn^{2+} seems more rugged than that of A$\beta_{(1–40)}$–Zn^{2+}. This suggests that the conformational conversion of A$\beta_{(1–40)}$–Zn^{2+} could take place more easily and frequently. Such result is in general agreement with recent experimental observations that A$\beta_{(1–42)}$–Zn^{2+} is more rigid than A$\beta_{(1–40)}$–Zn^{2+} [18]. Note that zinc-free A$\beta_{(1–42)}$ is also more rigid than A$\beta_{(1–42)}$ at the C terminus [72, 74, 86]. In summary, the above analyses show that the conformational spaces of Zn^{2+}-bound Aβ generated by REMD simulations provide sufficient targets for fishing by bifunctional molecules.

Binding interactions of Aβ–Zn^{2+} with bifunctional molecules

The final conformations of ligand–A$\beta_{(1–40)}$–Zn^{2+} selected by docking were shown in Fig. 4, along with corresponding docking energies summarized in Table 1. Interestingly, one conformation of A$\beta_{(1–40)}$–Zn^{2+} (conformer 28 of cluster 68) was found by docking that could accommodate three ligands (Fig. 4a). Moreover, diverse conformations of A$\beta_{(1–40)}$–Zn^{2+} were selected for each ligand (Fig. 4). Previous docking studies that used multiple conformations of both L2B and zinc-free A$\beta_{(1–40)}$ also found five potential conformations of A$\beta_{(1–40)}$ that showed distinct binding modes for L2B [55]. In addition, the corresponding docking energies obtained varied from -2.61 to -5.68 kcal/mol. Note that the docking energies for L2B with two A$\beta_{(1–40)}$–Zn^{2+} conformations were -5.66 and -5.73 kcal/mol in this work. Although these values represent the lowest binding energies predicted by docking studies, they need to be taken with caution because L2B was observed to dissociate from A$\beta_{(1–40)}$–Zn^{2+} in the subsequent MD simulations with explicit solvent model (Table 1). Hence, more candidate conformations of highly disordered Aβ are needed to screen its binding mode with small molecules. And the docking results require further validation via MD simulations, as the strategy proposed in this work.

The starting structures of ligand–A$\beta_{(1–40)}$–Zn^{2+} (ligand = HBX, MPY′, and L2B) (Fig. 4) were subjected to at least 30 ns classical MD simulations in aqueous solution. The nomenclature of each system, docking energies, as well as the simulations results are summarized in Table 1. The number of contacts between Aβ–Zn^{2+} and each ligand was monitored in order to test if each system has reached equilibrium (Fig. S3 and Fig. S4). A contact occurs when any atom of Aβ–Zn^{2+} within 4 Å of any atom of a ligand.

It was found that the formation of stable ligand–A$\beta_{(1–40)}$–Zn^{2+} complex failed for four systems. In particular, the same conformation of A$\beta_{(1–40)}$–Zn^{2+} selected by docking (Fig. 4a) seemed not suitable for HBX, L2B, and MPY′ (Fig. S3b, S3c, and S3e). Neither of two conformations of A$\beta_{(1–40)}$–Zn^{2+} with high docking energies was

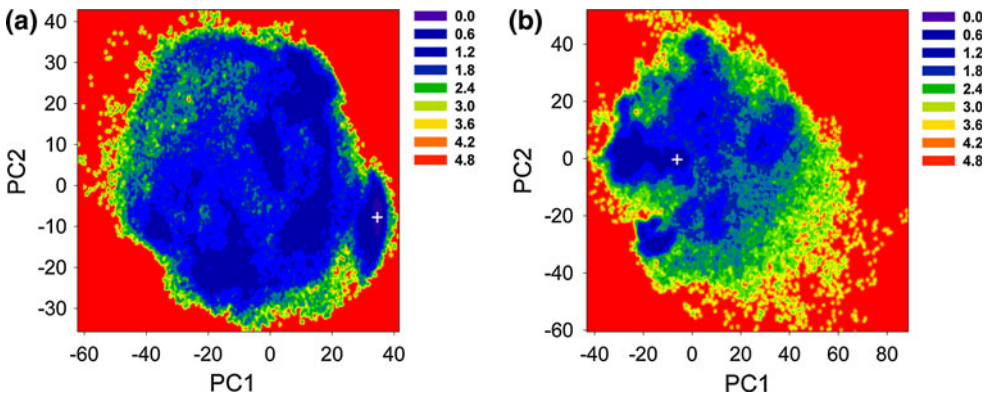

Fig. 3 Conformational free energy surfaces for A$\beta_{(1–40)}$–Zn^{2+} (**a**) and A$\beta_{(1–42)}$–Zn^{2+} (**b**) system (1:1 Zn^{2+}:Aβ molar ratio). Each was constructed by projecting its conformations onto the first two principle components (PC1 and PC2). The free energy values (in kcal/mol) were obtained by $\Delta G = -k_B T[\ln P_i - \ln P_{max}]$, where P_i and P_{max} are the probability distribution calculated from a histogram of individual REMD simulation trajectory. $\ln P_i - \ln P_{max}$ was used to ensure $\Delta G = 0$ for the lowest free energy points

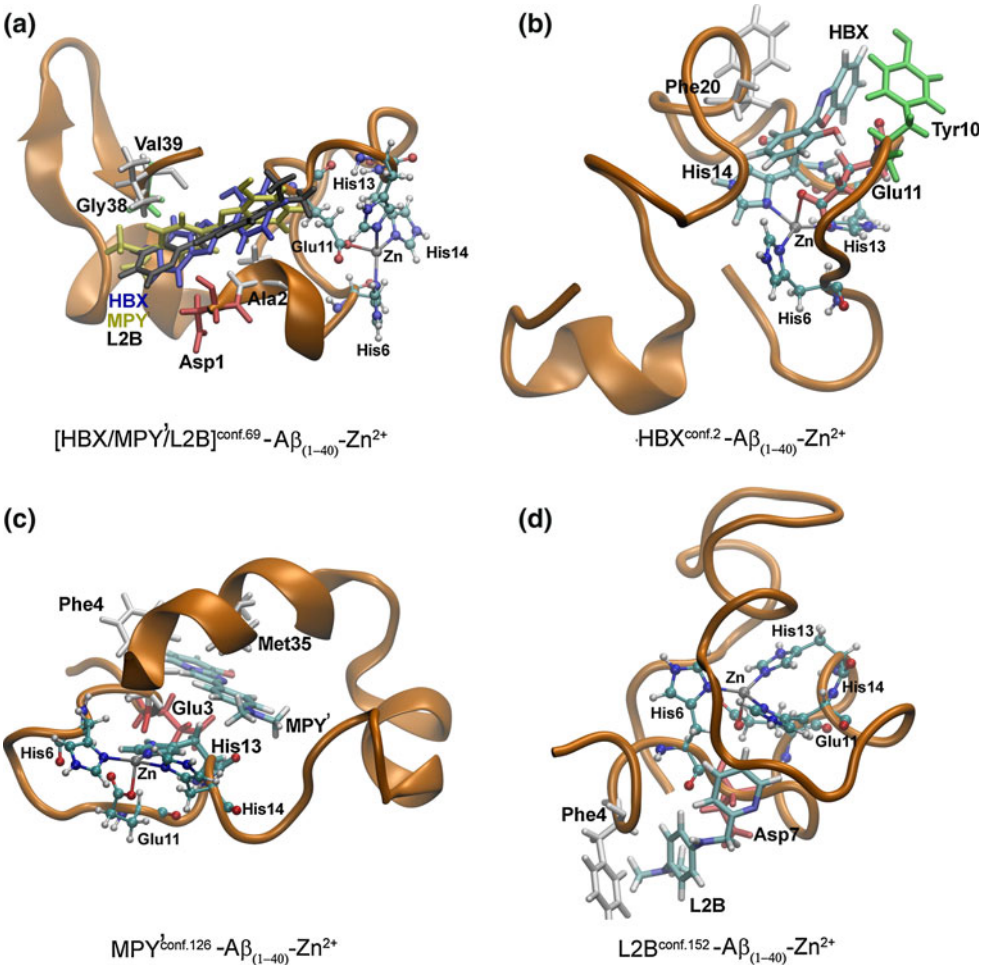

Fig. 4 The binding conformations of ligand–A$\beta_{(1-40)}$–Zn^{2+} (ligand = HBX, MPY′, and L2B) selected based on docking energies. Note that HBX, MPY′, and L2B share the same one conformation of A$\beta_{(1-40)}$–Zn^{2+} which is selected from the same cluster 69. Aβ is shown in New Cartoon representation. HBX, MPY′, L2B, and proximal residues of Aβ are displayed in Licorice representation. Zn^{2+} and its binding sites (His^6, Glu^{11}, His^{13}, and His^{14}) are displayed in CPK representation. Amino acids are colored based on residue types, basic in *blue*; acidic in *red*; polar in *green*; nonpolar or hydrophobic in *white*

suitable for L2B (Fig. 4d, Fig. S3c and S3d). This result are not unexpected given the fact that Aβ peptides are intrinsically disordered proteins. Similarly, the free energy profiles also revealed the polymorphic states of Zn^{2+}-bound Aβ (Fig. 3). Therefore, unlike those rigid macromolecules, the initial recognition of Aβ by small ligands requires more candidate conformations. Also note that the dissociation of ligand from Zn^{2+}-bound A$\beta_{(1-40)}$ can occur within 30 ns in MD simulations, indicating that either the ligand could not induce A$\beta_{(1-40)}$ toward a favorable binding conformation in a nanosecond time scale or no proper conformations were selected.

Two conformations of A$\beta_{(1-40)}$–Zn^{2+} from different clusters were identified to interact with HBX and MPY′, respectively (Fig. 4b, c, Fig. S3a and S3f). The number of contacts did not fluctuate too much after 30 ns in both cases, implying that HBX and MPY′ were capable of recognizing the corresponding conformations of A$\beta_{(1-40)}$–Zn^{2+} and establishing relatively stable interactions. Subsequently, the binding free energy was calculated for each system using the last 10-ns trajectory of MD simulations by MM/GBSA method (Table 1). Figure 5 shows the representative snapshots of the binding conformations of HBX–A$\beta_{(1-40)}$–Zn^{2+} and MPY′–A$\beta_{(1-40)}$–Zn^{2+}. Compared with the initial bound conformation (Fig. 4c), more hydrophobic residues of A$\beta_{(1-40)}$ are involved in the interactions with MPY′, including the typical central hydrophobic cluster (CHC, residues 17–21) (Fig. 5b) which contributes greatly to their binding affinity. Moreover, MPY′ was observed to interact with Val^{12} and His^{13} frequently, suggesting that MPY′ could chelate Zn^{2+} by interacting these residues that are close to metal binding sites (His^6, Glu^{11}, His^{13}, and His^{14}) of Aβ. It has been observed from NMR experiments that MPY′ may interact with metal binding sites in zinc-free A$\beta_{(1-40)}$ including Glu^{11} and His^{13}, however, interactions with CHC region of A$\beta_{(1-40)}$ were not so significant [54]. It appears that upon binding zinc, A$\beta_{(1-40)}$ may provide more preferred conformations that afford better hydrophobic interactions with MPY′. In contrast, less hydrophobic interactions are observed between HBX and A$\beta_{(1-40)}$–Zn^{2+} throughout the MD simulations (Figs. 4b, 5a), resulting in less favorable association.

The final conformations of ligand–A$\beta_{(1-42)}$–Zn^{2+} selected by docking are shown in Fig. 6. Note that different

Table 1 Summary of the systems studies in this work, their corresponding cluster number, docking energy, and free energy calculated by MM/GBSA method

System name	Cluster no.-confomer. no	AutoDock binding energy (kcal/mol)	Ligand dissociation	MM/GBSA binding free energy (kcal/mol)
$HBX^{conf.2}$–$A\beta_{(1-40)}$–Zn^{2+}	2-254	−6.29	No	−43.47 (1.54)
$HBX^{conf.69}$–$A\beta_{(1-40)}$–Zn^{2+}	69-28	−6.63	Yes	–
$MPY'^{conf.69}$–$A\beta_{(1-40)}$–Zn^{2+}	69-28	−6.40	Yes	–
$MPY'^{conf.126}$–$A\beta_{(1-40)}$–Zn^{2+}	126-20	−6.43	No	−60.63 (0.82)
$L2B^{conf.69}$–$A\beta_{(1-40)}$–Zn^{2+}	69-28	−5.73	Yes	–
$L2B^{conf.152}$–$A\beta_{(1-40)}$–Zn^{2+}	152-14	−5.66	Yes	–
$HBX^{conf.2}$–$A\beta_{(1-42)}$–Zn^{2+}	2-66	−6.23	No	−14.71 (0.36)
$HBX^{conf.101}$–$A\beta_{(1-42)}$–Zn^{2+}	101-7	−6.45	No	−1.75 (0.22)
$MPY'^{conf.6}$–$A\beta_{(1-42)}$–Zn^{2+}	6-228	−6.17	No	−8.59 (2.27)
$MPY'^{conf.101}$–$A\beta_{(1-42)}$–Zn^{2+}	101-28	−6.27	Yes	–
$L2B^{conf.66}$–$A\beta_{(1-42)}$–Zn^{2+}	66-39	−5.52	No	−20.63 (0.78)
$L2B^{conf.101}$–$A\beta_{(1-42)}$–Zn^{2+}	101-3	−5.61	Yes	–

The standard deviations were calculated using block average method

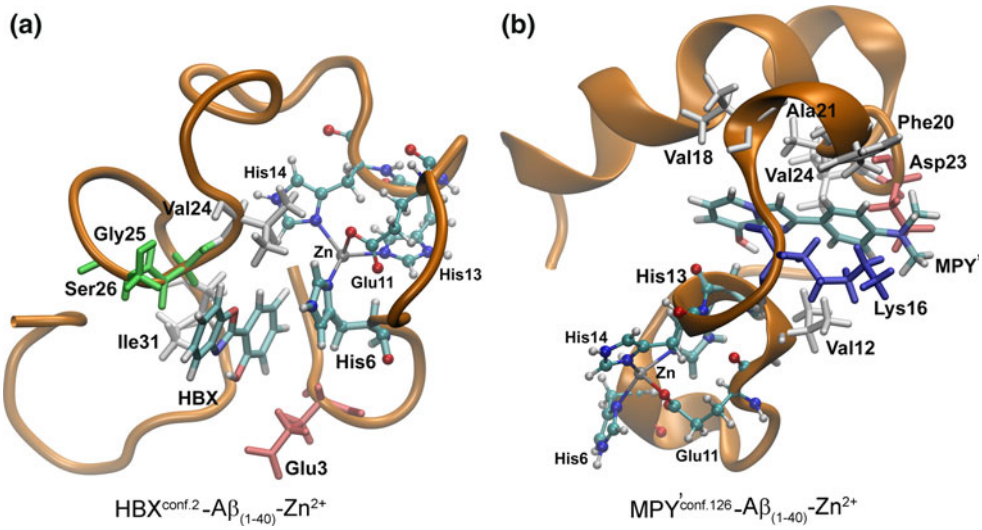

Fig. 5 The representative conformations of $A\beta_{(1-40)}$–Zn^{2+} which show relatively high binding affinity to HBX and MPY′. These snapshots are taken from classical MD simulations of $A\beta_{(1-40)}$–Zn^{2+} with HBX and MPY′ molecules in aqueous solution. The representations are the same as in Fig. 4

conformations of $A\beta_{(1-42)}$–Zn^{2+} from the same cluster (cluster 101) were identified to host different ligands (Fig. 6b, d, f). The number of contacts between $A\beta_{(1-42)}$–Zn^{2+} and different ligands (Fig. S4) shows that the conformations of $A\beta_{(1-42)}$–Zn^{2+} from the same cluster (cluster 101) are unfavorable to L2B (Fig. S4d) and MPY′ (Fig. S4f), whereas display very low binding affinity to HBX (Fig. S4b). This observation is in line with the corresponding binding free energies (Table 1). Apparently, the recognition of $A\beta_{(1-42)}$–Zn^{2+} by these bifunctional molecules is dependent on the initial selected conformations of $A\beta_{(1-42)}$–Zn^{2+}. The docking positions of HBX, MPY′, and L2B are primarily in the flexible loop region from Leu^{17} to the C-terminus of $A\beta_{(1-42)}$ (Fig. 6b, d, f), but their binding interactions induce the conformations of $A\beta_{(1-42)}$ into diverse substates that are not preferred to accommodate HBX, MPY′ and L2B.

On the contrary, except MPY′ (Fig. S4e), HBX (Fig. S4a) and L2B (Fig. S4c) strongly interact with several conformations of $A\beta_{(1-42)}$–Zn^{2+} that are chosen from different clusters (Fig. S4a, S4c, and S4e). The average root-mean-square deviations (RMSDs) of $A\beta_{(1-42)}$ relative to their initial conformations in the system of HBX–$A\beta_{(1-42)}$–Zn^{2+} and L2B–$A\beta_{(1-42)}$–Zn^{2+} are about 3.0 and 2.8 Å, respectively (Figs. 6a, e, 7). The results discussed above implicate that the conformations that are responsible for binding bifunctional molecules could have already existed in the conformational ensemble of $A\beta$–Zn^{2+}. Given the polymorphic states of $A\beta$–Zn^{2+}, the selection of proper conformations by these small molecules could be achieved through multiple pathways of various specificity efficiently. Therefore, no common binding modes can be expected. Similar to $A\beta_{(1-40)}$–Zn^{2+} systems, in the case of $A\beta_{(1-42)}$–Zn^{2+} interacting with L2B (Fig. 7b), the

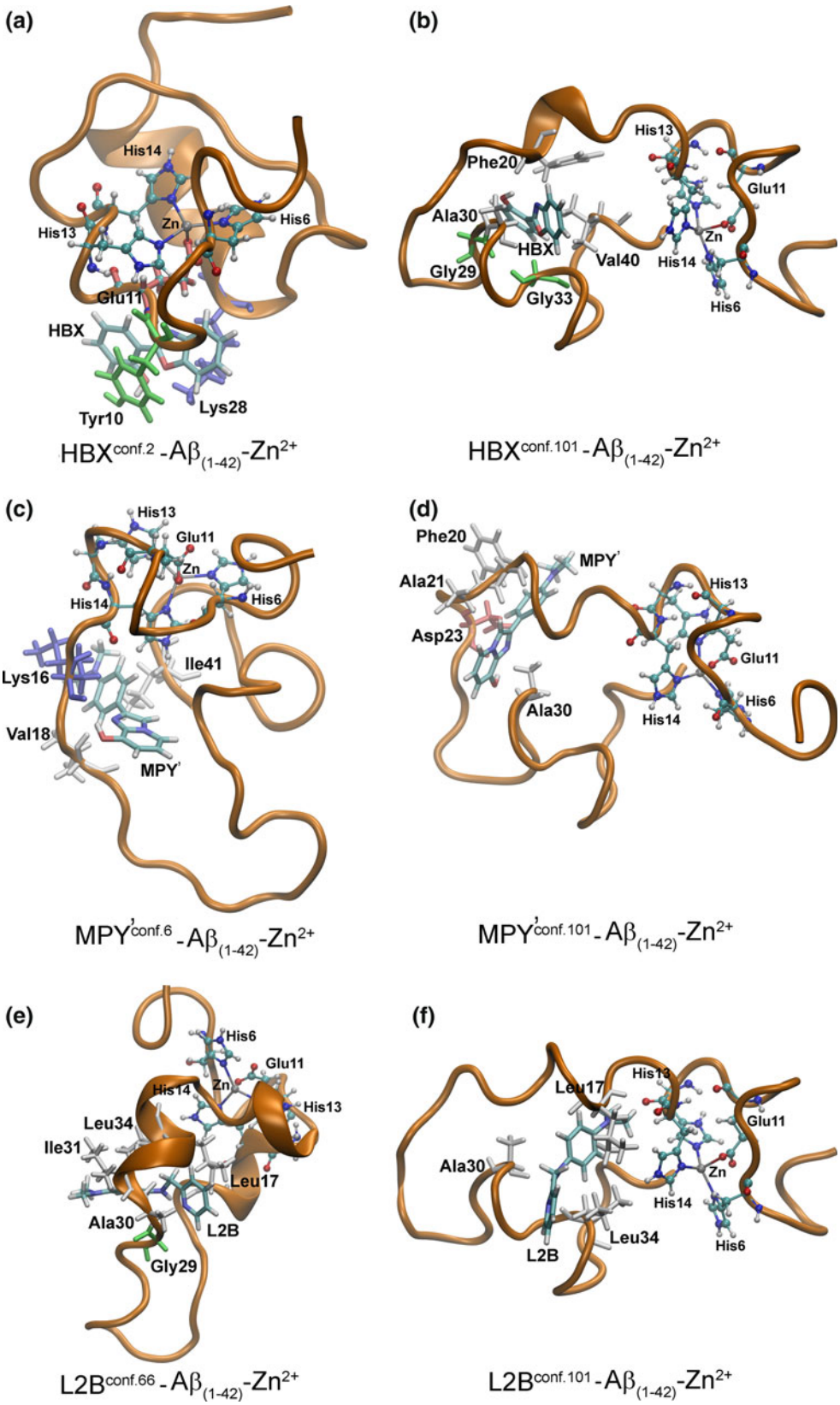

Fig. 6 The binding conformations of ligand–$A\beta_{(1-42)}$–Zn^{2+} (ligand = HBX, MPY′, and L2B) selected based on docking energies. Note that HBX, MPY′ and L2B recognize different conformations of $A\beta_{(1-42)}$–Zn^{2+} that are selected from the same cluster 101. The representations are the same as in Fig. 4

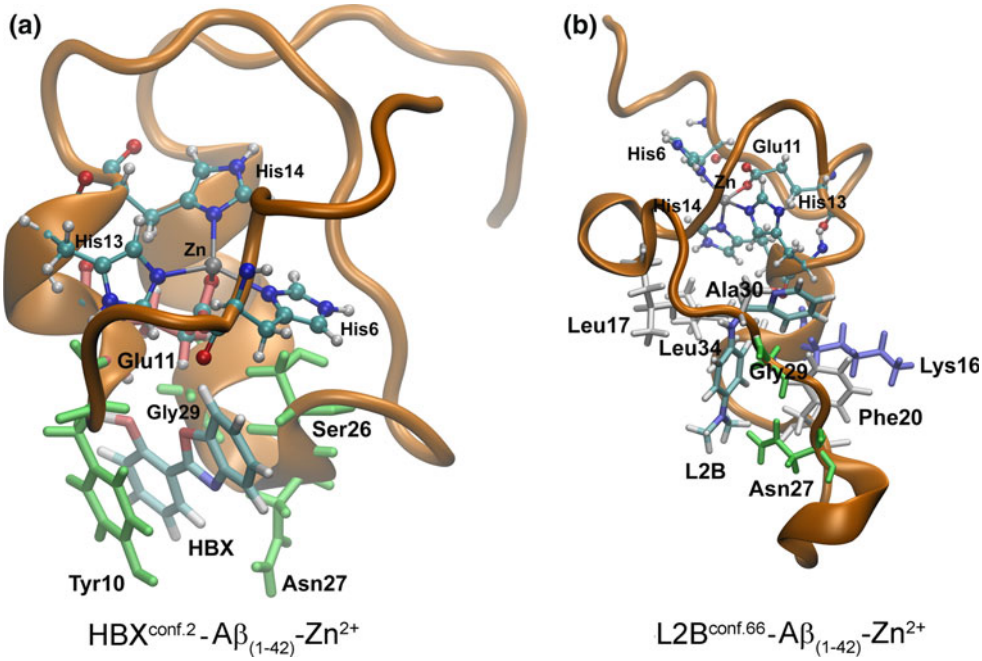

Fig. 7 The representative conformations of A$\beta_{(1-42)}$–Zn^{2+} which show relatively high binding affinity to HBX and L2B. These snapshots are taken from the classical MD simulations of A$\beta_{(1-42)}$–Zn^{2+} with HBX and L2B molecules in aqueous solution. The representations are the same as in Fig. 4

favorable binding site for L2B involves residues in the CHC such as Leu^{17} and Phe^{20}. Other hydrophobic residues like Ala^{30} and Leu^{34} are also identified to participate in the whole binding process (Fig. 7b). This finding, together with the results obtained from the system MPY′–A$\beta_{(1-40)}$–Zn^{2+} as discussed above, highlight the important role of the CHC of Aβ in the recognition of bifunctional molecules. It has been suggested that the two hydrophobic regions (Leu^{17}-Ala^{21} and Ile^{31}-Val^{36}) of full-length Aβ peptides are prone to promote Aβ aggregation [87–89]. Inhibitors that interfere with these regions may therefore act as potential therapeutic agents for the treatment of AD. Our results indicate that the binding of bifunctional molecules in these regions could prevent Aβ oligomerization and aggregation by reducing the hydrophobic contacts between Aβ peptides.

Apart from hydrophobic interactions, the polar interactions contributed by Lys^{16} were found in MPY′–A$\beta_{(1-40)}$–Zn^{2+} and L2B–A$\beta_{(1-42)}$–Zn^{2+} systems. Importantly, His^{13} was observed to be proximal to L2B over the entire MD simulations (Fig. 7b). Such finding is also consistent with experimental evidence which suggests that Glu^{11} and His^{13} of Aβ closely contact with L2B in solution [55]. However, Glu^{11} was only identified to interact with HBX in two sets MD simulations where HBX showed relatively lower binding affinity for Aβ peptides (Figs. 5a and 7a).

The propensity for the secondary structures of Aβ was also calculated for those residues that interact with bifunctional molecules. As shown in Fig. 8 (also see Figs. 5, 7), those residues that have stable contacts (high probability) with a ligand tend to form bend, turn, 3_{10}-helix, and random coil structures. This observation suggests that the conformational change of Aβ induced by a small ligand upon association would become much easier if the initial binding conformations adopt more flexible secondary structures.

It is worth noting that due to the additional Ile^{41} and Ala^{42} at the C-terminus, A$\beta_{(1-40)}$ and A$\beta_{(1-42)}$ display different structural properties in the form of monomers [72, 74, 86, 87, 90], soluble oligomers [91, 92], and fibrils which show similar protofilament structures [93] but distinct molecular recycling [94]. It is thus reasonably expected that Zn^{2+}-bound A$\beta_{(1-40)}$ and A$\beta_{(1-42)}$ exhibit different conformational ensemble (Figs. 2, 3). Their different propensity for various bifunctional molecules could be of interest. However, there is no direct experimental evidence that shows discernable difference between A$\beta_{(1-40)}$ and A$\beta_{(1-42)}$ in the recognition of small molecules with or without metal ions. Our results show that both Zn^{2+}-bound Aβ peptides can adopt various binding conformations, and the interactions with C-terminal residues contribute little to the binding affinity (see Fig. 8). This finding implies that the effect of the two hydrophobic residues (Ile^{41} and Ala^{42}) on the recognition of small molecules is not so significant.

MD simulations of HBX, MPY′ and L2B with free Zn^{2+} in aqueous solution shown that they were capable of chelating zinc ions (Fig. S5). The average distance between Zn^{2+} binding sites of HBX and Zn^{2+} were 2.27 and 2.11 Å. To further explore Zn^{2+} binding properties of bifunctional molecules that can interact with Aβ peptides, the distances between Zn^{2+} binding sites of these molecules and Aβ-bound

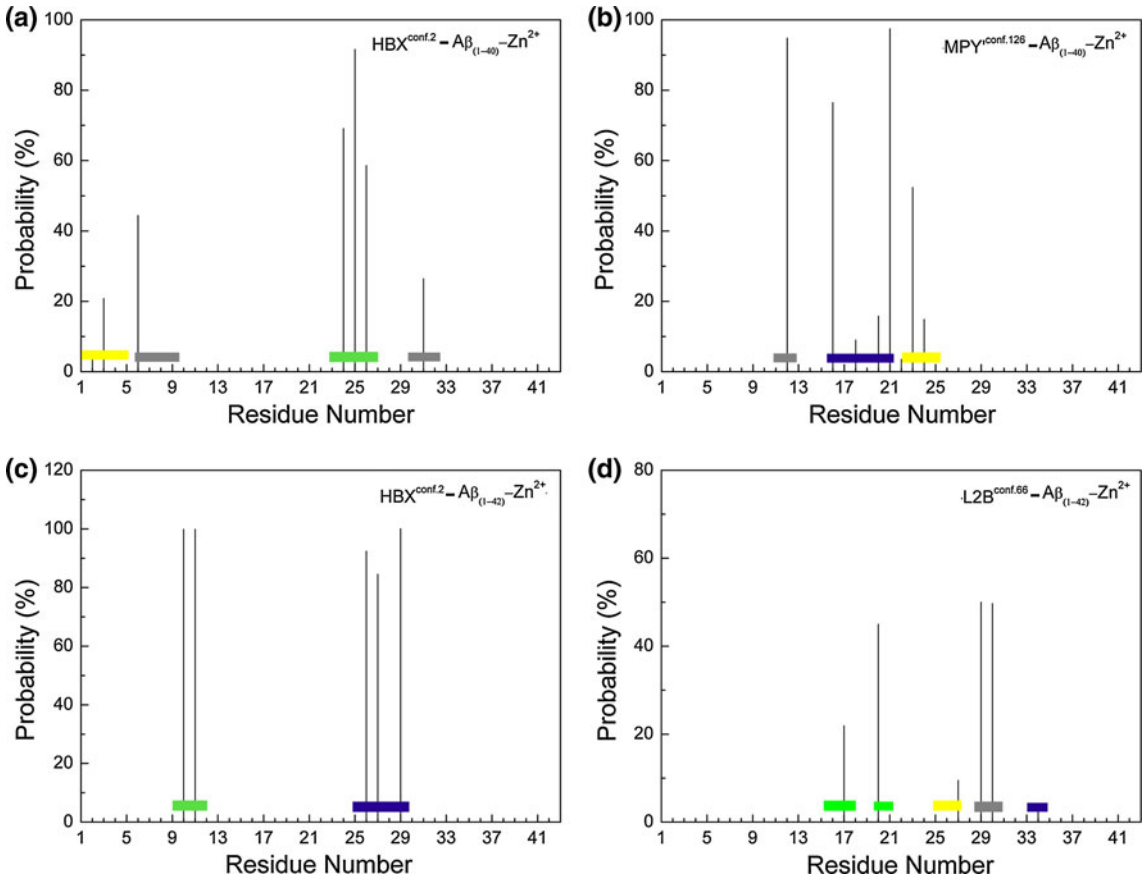

Fig. 8 The probability of contacts between Aβ–Zn^{2+} and bifunctional molecules. The type of secondary structures is shown for the binding residues in different colors: yellow for trun, *grey* for random coil, *green* for bend, and *blue* for 3_{10}-helix

Zn^{2+} were calculated and depicted in Fig.S6. The average distance ranged from 8.11 to 10.47 Å, demonstrating that they could not directly interact with Zn^{2+} surrounded by Aβ. This finding is different from the studies of Choi et al. [55] where they suggested that L2B was able to be in contact with both Aβ and Zn^{2+} and proposed a Aβ–Zn^{2+}–L2B complex that was important for controlling metal-induced Aβ aggregation. From our studies, it seems more possible that bifunctional molecules first reduce Aβ binding affinity for Zn^{2+} by interfering with Aβ, followed by sequestering Zn^{2+} out from Zn^{2+}–Aβ complex. However, due to the polymorphic state of Aβ, its binding affinity for Zn^{2+} should vary with different coordination environments. Moreover, the recognition of Zn^{2+}–Aβ with these ligands requires selection of appropriate conformations of Zn^{2+}–Aβ. As a result, the extraction of Zn^{2+} from Aβ by these molecules could be prevented if the interactions between bifunctional molecules and Aβ (Glu^{11} and His^{13}, in particular) are weaker than the binding affinity of Aβ for Zn^{2+}. This two-stage mechanism provides a reasonable explanation for the experimental observation that L2B could interact with Aβ but not chelate metal ions completely [55]. Whereas the formation of Aβ–Zn^{2+}–L2B structure could be regarded as a rare event where Aβ provides enough open position for L2B to contact with Zn^{2+}. Overall, our MD simulations reveal that the formation of ligand–Aβ–Zn^{2+} structure is more preferred than the formation of Aβ–Zn^{2+}-ligand structure.

Binding free energy between Aβ–Zn^{2+} and bifunctional molecules

The contribution of enthalpy and entropy to the binding free energy was calculated for the four systems that show higher binding affinities (Fig. 9). Interestingly, although the averaged binding free energy varies from -14.71 to -60.63 kcal/mol, there is no significant difference in their entropy values whereas enthalpy contributes to the differing binding free energies. This finding suggests that the association of Aβ–Zn^{2+} with bifunctional molecules is an enthalpy-driven process. In particular, the VDW interactions between $A\beta_{(1–40)}$–Zn^{2+} and hydrophobic molecules (HBX and MPY′) favor their association by about −22.56 and

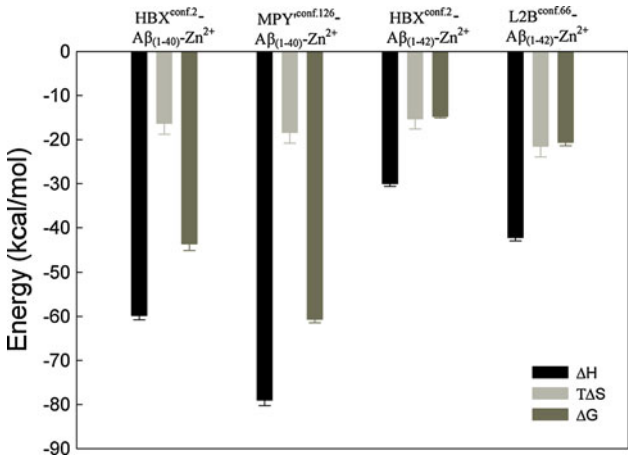

Fig. 9 The energy contributions to the binding free energies between Aβ–Zn^{2+} and bifunctional molecules

−32.33 kcal/mol, respectively. The solvation energies for the binding of A$\beta_{(1–40)}$–Zn^{2+} with HBX and MPY′ are -39.64 and -37.62 kcal/mol, accounting for 66 and 48 % of the total enthalpy, respectively. Taken together, the preferred enthalpy suggests that hydrophobic interactions between these bifunctional molecules and Aβ (CHC regions) are crucial for their recognition and association (Fig. 8). Therefore, it seems desirable to design novel bifunctional molecules by introduction of more hydrophobic moieties like bulky aromatic rings into their structure.

Conclusions

The combination of molecular docking and MD simulations has already been recognized as a valuable tool in drug design [95]. In this work, a more integrated strategy was proposed to investigate the binding mode of zinc-bound Aβ monomers with three bifunctional small molecules. Given the dynamic property of zinc-bound Aβ, the recognition of Aβ by small molecules is more like a stochastic process. Therefore, extensive REMD simulations were carried out to sample the conformational spaces of zinc-bound Aβ peptides. No significant difference of binding modes was observed between A$\beta_{(1–40)}$–Zn^{2+} and A$\beta_{(1–42)}$–Zn^{2+} although they show different conformational ensemble. Target-fishing using docking was performed to select potential binding conformations that were further tested by MD simulations and free energy calculations. The binding sites in the conformations of Aβ–Zn^{2+} that preferentially interact with bifunctional molecules involve two hydrophobic regions (Leu^{17}-Ala^{21} and Ile^{31}-Val^{36}). Recent MD simulations on the interactions of Aβ monomer and oligomer with some potential drugs also highlight the important role of these hydrophobic cores [96]. Taken together, our results indicate that the hydrophobic region of Aβ could act as a major target for designing new bifunctional AD drugs.

In line with the conformational selection model in biomolecular recognition, it is important to note that Aβ–Zn^{2+} could adopt various conformations upon ligand association whereas the binding sites prefer to adopt flexible secondary structures. The binding process is primarily driven by enthalpy and characterized by favorable hydrophobic interactions. Importantly, a two-step mechanism emerged from this study, which suggests that bifunctional small molecules first interact with metal-bound Aβ and disrupt Aβ affinity for metal ions, then function as metal chelators. In summary, our study provides detailed mechanistic insights into how bifunctional molecules interact with zinc-bound Aβ peptides. The integrated approach used in this study could also be helpful for the design of novel drugs for AD.

Acknowledgments We are grateful to Dr. Orkid Coskuner-Weber (The University of Texas at San Antonio, USA) for critical comments of this research. Computations were performed on the clusters at the High-Performance Computing Center of Dalian University of Technology. This work is supported by the Major State Basic Research Development Program (Grant No. 200900376). Dr. Xu and Dr. Bao thanks financial support from the Fundamental Research Funds for the Central Universities (grant No. DUT12LK38 and DUT11SM01).

References

1. Hardy J, Selkoe DJ (2002) The amyloid hypothesis of Alzheimer's disease: progress and problems on the road to therapeutics. Science 297:353–356
2. Jakob-Roetne R, Jacobsen H (2009) Alzheimer's disease: from pathology to therapeutic approaches. Angew Chem Int Ed 48:3030–3059
3. Karran E, Mercken M, De Strooper B (2011) The amyloid cascade hypothesis for Alzheimer's disease: an appraisal for the development of therapeutics. Nat Rev Drug Discov 10:698–712
4. Straub JE, Thirumalai D (2011) Toward a molecular theory of early and late events in monomer to amyloid fibril formation. Ann Rev Phys Chem 62:437–463
5. Perry G, Cash AD, Srinivas R, Smith MA (2002) Metals and oxidative homeostasis in Alzheimer's disease. Drug Dev Res 56:293–299
6. Bush AI (2003) The metallobiology of Alzheimer's disease. Trends Neurosci 26:207–214
7. Maynard CJ, Bush AI, Masters CL, Cappai R, Li QX (2005) Metals and amyloid-beta in Alzheimer's disease. Int J Exp Pathol 86:147–159
8. Shcherbatykh I, Carpenter DO (2007) The role of metals in the etiology of Alzheimer's disease. J Alzheimers Dis 11:191–205
9. Bush AI, Tanzi RE (2008) Therapeutics for Alzheimer's disease based on the metal hypothesis. Neurotherapeutics 5:421–432
10. Chiang PK, Lam MA, Luo Y (2008) The many faces of amyloid β in Alzheimer's disease. Curr Mol Med 8:580–584
11. Miura T, Suzuki K, Kohata N, Takeuchi H (2000) Metal binding modes of Alzheimer's amyloid β-peptide in insoluble aggregates and soluble complexes. Biochemistry 39:7024–7031
12. Kozin SA, Zirah S, Rebuffat S, Hoa GH, Debey P (2001) Zinc binding to Alzheimer's Aβ(1–16) peptide results in stable soluble complex. Biochem Biophys Res Commun 285:959–964

13. Minicozzi V, Stellato F, Comai M, Dalla Serra M, Potrich C, Meyer-Klaucke W, Morante S (2008) Identifying the minimal copper- and zinc-binding site sequence in amyloid-β peptides. J Biol Chem 283:10784–10792
14. Faller P, Hureau C (2009) Bioinorganic chemistry of copper and zinc ions coordinated to amyloid-β peptide. Dalton Trans 21:1080–1094
15. Faller P (2009) Copper and zinc binding to amyloid-β: coordination dynamics aggregation reactivity and metal-ion transfer. ChemBioChem 10:2837–2845
16. Tõugu V, Tiiman A, Palumaa P (2011) Interactions of Zn(II) and Cu(II) ions with Alzheimer's amyloid-β peptide Metal ion binding contribution to fibrillization and toxicity. Metallomics 3:250–261
17. Watt NT, Whitehouse IJ, Hooper NM (2011) The role of zinc in Alzheimer's disease. Int J Alzheimers Dis 2011:971021–971030
18. Rezaei-Ghaleh N, Giller K, Becker S, Zweckstetter M (2011) Effect of zinc binding on β-amyloid structure and dynamics: implications for Aβ aggregation. Biophys J 101:1202–1211
19. Zirah S, Kozin SA, Mazur AK, Blond A, Cheminant M, Ségalas-Milazzo I, Debey P, Rebuffat S (2006) Structural changes of region 1–16 of the Alzheimer disease amyloid β-peptide upon zinc binding and in vitro aging. J Biol Chem 281:2151–2161
20. Tsvetkov PO, Kulikova AA, Golovin AV, Tkachev YV, Archakov AI, Kozin SA, Makarov AA (2010) Minimal Zn^{2+} binding site of amyloid-β. Biophys J 99:L84–L86
21. Mekmouche Y, Coppel Y, Hochgräfe K, Guilloreau L, Tallmard C, Mazarguil H, Faller P (2005) Characterization of the ZnII binding to the peptide amyloid-β1–16 linked to Alzheimer's disease. ChemBioChem 6:1663–1671
22. Gaggelli E, Janicka-Klos A, Jankowska E, Kozlowski H, Migliorini C, Molteni E, Valensin D, Valensin G, Wieczerzak E (2008) NMR studies of the Zn2 + interactions with rat and human β-amyloid (1–28) peptides in water-micelle environment. J Phys Chem B 112:100–109
23. Furlan S, La Penna G (2009) Modeling of the Zn2 + binding in the 1–16 region of the amyloid β peptide involved in Alzheimer's disease. Phys Chem Chem Phys 11:6468–6481
24. Karr JW, Kaupp LJ, Szalai VA (2004) Amyloid-β binds Cu^{2+} in a mononuclear metal ion binding site. J Am Chem Soc 126:13534–13538
25. Kowalik-Jankowska T, Ruta M, Wisniewska K, Lankiewicz L (2003) Coordination abilities of the 1–16 and 1–28 fragments of β-amyloid peptide towards copper(II) ions: a combined potentiometric and spectroscopic study. J Inorg Biochem 95:270–282
26. Ma QF, Hu J, Wu WH, Liu HD, Du JT, Fu Y, Wu YW, Lei P, Zhao YF, Li YM (2006) Characterization of copper binding to the peptide amyloid-β(1–16) associated with Alzheimer's disease. Biopolymers 83:20–31
27. Baruch-Suchodolsky R, Fischer B (2008) Soluble amyloid β_{1-28}-copper(I)/copper(II)/iron(II) complexes are potent antioxidants in cell-free systems. Biochemistry 47:7796–7806
28. Gaggelli E, Grzonka Z, Kozlowski H, Migliorini C, Molteni E, Valensin D, Valensin G (2008) Structural features of the Cu(II) complex with the rat Aβ(1-28) fragment. Chem Commnu 341–343
29. Shin BK, Saxena S (2008) Direct evidence that all three histidine residues coordinate to Cu(II) in amyloid-β_{1-16}. Biochemistry 47:9117–9123
30. Pedersen JT, Teilum K, Heegaard NHH, Østergaard J, Adolph HW, Hemmingsen L (2011) Rapid formation of a preoligomeric peptide-metal-peptide complex following copper(II) binding to Amyloid β peptides. Angew Chem Int Ed 50:2532–2535
31. Miller Y, Ma B, Nussinov R (2010) Polymorphism in Alzheimer Aβ amyloid organization reflects conformational selection in a rugged energy landscape. Chem Rev 110:4820–4838
32. Colletier JP, Laganowsky A, Landau M, Zhao M, Soriaga AB, Goldschmidt L, Flot D, Cascio D, Sawaya MR, Eisenberg D (2011) Molecular basis for amyloid-β polymorphism. Proc Natl Acad Sci USA 108:16938–16943
33. Yu X, Zheng J (2011) Polymorphic structures of Alzheimer's β-amyloid globulomers. PLoS One 6:e20575
34. Miller Y, Ma B, Nussinov R (2010) Zinc ions promote Alzheimer Aβ aggregation via population shift of polymorphic states. Proc Natl Acad Sci USA 107:9490–9495
35. Parthasarathy S, Long F, Miller Y, Xiao Y, McElheny D, Thurber K, Ma B, Nussinov R, Ishii Y (2011) Molecular-level examination of Cu^{2+} binding structure for amyloid fibrils of 40-residue Alzheimer's β by solid-state NMR spectroscopy. J Am Chem Soc 133:3390–3400
36. Ricchelli F, Drago D, Filippi B, Tognon G, Zatta P (2005) Aluminum-triggered structural modifications and aggregation of β-amyloids. Cell Mol Life Sci 62:1724–1733
37. Miller Y, Ma B, Nussinov R (2012) Metal binding sites in amyloid oligomers: Complexes and mechanisms. Coord Chem Rev. doi:10.1016/j.ccr.2011.12.022
38. Cohen T, Frydman-Marom A, Rechter M, Gazit E (2006) Inhibition of amyloid fibril formation and cytotoxicity by hydroxyindole derivatives. Biochemistry 45:4727–4735
39. Yadav A, Sonker M (2009) Perspectives in designing anti aggregation agents as Alzheimer disease drugs. Eur J Med Chem 44:3866–3873
40. Kim S, Chang WE, Kumar R, Klimov DK (2011) Naproxen interferes with the assembly of Aβ oligomers implicated in Alzheimer's disease. Biophys J 100:2024–2032
41. Schütz AK, Soragni A, Hornemann S, Aguzzi A, Ernst M, Böckmann A, Meier BH (2011) The amyloid-Congo red interface at atomic resolution. Angew Chem Int Ed 50:5956–5960
42. Sood A, Abid M, Sauer C, Hailemichael S, Foster M, Török B, Török M (2011) Disassembly of preformed amyloid beta fibrils by small organofluorine molecules. Bioorg Med Chem Lett 21:2044–2047
43. Shiri S, Michal L, Anat F, Yaniv A, Roni S, Ludmila B, Ehud G, Hanoch S (2011) Quantitative structure–activity relationship analysis of β-amyloid aggregation inhibitors. J Comput Aided Mol Des 25:135–144
44. Viet MH, Ngo ST, Lam NS, Li MS (2011) Inhibition of aggregation of amyloid peptides by beta-sheet breaker peptides and their binding affinity. J Phys Chem B 115:7433–7446
45. Urbanc B, Betnel M, Cruz L, Li H, Fradinger EA, Monien BH, Bitan G (2011) Structural basis for Aβ 1–42 toxicity inhibition by Aβ C-terminal fragments: discrete molecular dynamics study. J Mol Biol 410:316–328
46. Yoo SI, Yang M, Brender JR, Subramanian V, Sun K, Joo NE, Jeong SH, Ramamoorthy A, Kotov NA (2011) Inhibition of amyloid peptide fibrillation by inorganic nanoparticles: functional similarities with proteins. Angew Chem Int Ed 50:5110–5115
47. Finefrock AE, Bush AI, Doraiswamy PM (2003) Current status of metals as therapeutic targets in Alzheimer's disease. J Am Geriatr Soc 51:1143–1148
48. Bush AI (2008) Drug development based on the metals hypothesis of Alzheimer's disease. J Alzheimers Dis 15:223–240
49. Hider RC, Ma YM, Molina-Holgado F, Gaeta A, Roy S (2008) Iron chelation as a potential therapy for neurodegenerative disease. Biochem Soc Trans 36:1304–1308
50. Perez LR, Franz KJ (2010) Minding metals: tailoring multifunctional chelating agents for neurodegenerative disease. Dalton Trans 39:2177–2187
51. Rodríguez-Rodríguez C, de Groot NS, Rimola A, Álvarez-Larena A, Lloveras V, Vidal-Gancedo J, Ventura S, Vendrell J, Sodupe M, González-Duarte P (2009) Design selection and characterization of thioflavin-based intercalation compounds with metal

chelating properties for application in Alzheimer's disease. J Am Chem Soc 131:1436–1451
52. Mancino AM, Hindo SS, Kochi A, Lim MH (2009) Effects of clioquinol on metal-triggered amyloid-β aggregation revisited. Inorg Chem 48:9596–9598
53. Braymer JJ, Detoma AS, Choi JS, Ko KS, Lim MH (2011) Recent development of bifunctional small molecules to study metal-amyloid-β species in Alzheimer's disease. Int J Alzheimers Dis 2011:623051–623060
54. Hindo SS, Mancino AM, Braymer JJ, Liu Y, Vivekanandan S, Ramamoorthy A, Lim MH (2009) Small molecule modulators of copper-induced Abeta aggregation. J Am Chem Soc 131:16663–16665
55. Choi JS, Braymer JJ, Nanga RPR, Ramamoorthy A, Lim MH (2010) Design of small molecules that target metal-Aβ species and regulate metal-induced Aβ aggregation and neurotoxicity. Proc Natl Acad Sci USA 107:21990–21995
56. Wu WH, Lei P, Liu Q, Hu J, Gunn AP, Chen MS, Rui YF, Su XY, Xie ZP, Zhao YF, Bush AI, Li YM (2008) Sequestration of copper from β-amyloid promotes selective lysis by cyclen-hybrid cleavage agents. J Biol Chem 283:31657–31664
57. Jensen M, Canning A, Chiha S, Bouquerel P, Pedersen JT, Østergaard J, Cuvillier O, Sasaki I, Hureau C, Faller P (2012) Inhibition of Cu-amyloid-β by using bifunctional peptides with β-sheet breaker and chelator moieties. Chem Eur J 18:4836–4839
58. Dedeoglu A, Cormier K, Payton S, Tseitlin KA, Kremsky JN, Lai L, Li XH, Moir RD, Tanzi RE, Bush AI, Kowall NW, Rogers JT, Huang XD (2004) Preliminary studies of a novel bifunctional metal chelator targeting Alzheimer's amyloidogenesis. Expl Gerontol 39:1641–1649
59. Boehr DD, Nussinov R, Wright PE (2009) The role of dynamic conformational ensembles in biomolecular recognition. Nat Chem Biol 5:789–796
60. Sugita Y, Okamoto Y (1999) Replica-exchange molecular dynamics method for protein folding. Chem Phys Lett 314:141–151
61. Mitsutake A, Sugita Y, Okamoto Y (2001) Generalized-ensemble algorithms for molecular simulations of biopolymers. Biopolymers 60:96–123
62. Morris GM, Goodsell DS, Halliday RS, Huey R, Hart WE, Belew RK, Olson AJ (1998) Automated docking using a Lamarckian genetic algorithm and an empirical binding free energy function. J Comput Chem 19:1639–1662
63. Huey R, Morris GM, Olson AJ, Goodsell DS (2007) A semi-empirical free energy force field with charge-based desolvation. J Comput Chem 28:1145–1152
64. Kollman PA, Massova I, Reyes C, Kuhn B, Huo SH, Chong L, Lee M, Lee T, Duan Y, Wang W, Donini O, Cieplak P, Srinivasan J, Case DA, Cheatham TE (2000) Calculating structures and free energies of complex molecules: combining molecular mechanics and continuum models. Acc Chem Res 33:889–897
65. Hoops SC, Anderson KW, Merz KM (1991) Force-field design for metalloproteins. J Am Chem Soc 113:8262–8270
66. Peters MB, Yang Y, Wang B, Füsti-Molnár L, Weaver MN, Merz KM Jr (2010) Structural survey of zinc containing proteins and the development of the zinc AMBER force field (ZAFF). J Chem Theory Comput 6:2935–2947
67. Lin F, Wang RX (2010) Systematic derivation of AMBER force field parameters applicable to zinc-containing systems. J Chem Theory Comput 6:1852–1870
68. Wang JM, Cieplak P, Kollman PA (2000) How well does a restrained electrostatic potential (RESP) model perform in calculating conformational energies of organic and biological molecules? J Comput Chem 21:1049–1074
69. Lührs T, Ritter C, Adrian M, Riek-Loher D, Bohrmann B, Döeli H, Schubert D, Riek R (2005) 3D structure of Alzheimer's amyloid-β(1–42) fibrils. Proc Natl Acad Sci USA 102:17342–17347
70. Li WF, Zhang J, Su Y, Wang J, Qin M, Wang W (2007) Effects of zinc binding on the conformational distribution of the amyloid-β peptide based on molecular dynamics simulations. J Phys Chem B 111:13814–13821
71. Miller Y, Ma BY, Nussinov R (2011) The unique Alzheimer's β-amyloid triangular fibril has a cavity along the fibril axis under physiological conditions. J Am Chem Soc 133:2742–2748
72. Yang MF, Teplow DB (2008) Amyloid β-protein monomer folding: free-energy surfaces reveal alloform-specific differences. J Mol Biol 384:450–464
73. Sgourakis NG, Merced-Serrano M, Boutsidis C, Drineas P, Du ZM, Wang CY, Garcia AE (2011) Atomic-level characterization of the ensemble of the Aβ(1–42) Monomer in water using unbiased molecular dynamics simulations and spectral algorithms. J Mol Biol 405:570–583
74. Sgourakis NG, Yan YL, McCallum SA, Wang CY, Garcia AE (2007) The Alzheimer's peptides Aβ 40 and 42 adopt distinct conformations in water: a combined MD/NMR study. J Mol Biol 368:1448–1457
75. Jang S, Shin S (2006) Amyloid β-peptide oligomerization in silico: dimer and trimer. J Phys Chem B 110:1955–1958
76. Case DA, Darden TA, Cheatham III TE, Simmerling CL, Wang J, Duke RE, Luo R, Walker RC, Zhang W, Merz KM, Roberts BP, Wang B, Hayik S, Roitberg A, Seabra G, Kolossvai I, Wong KF, Paesani F, Vanicek J, Liu J, Wu X, Brozell SR, Steinbrecher T, Gohlke H, Cai Q, Ye X, Wang J, Hsieh MJ, Cui G, Roe DR, Mathews DH, Seetin MG, Sagui C, Babin V, Luchko T, Gusarov S, Kovalenko A, Kollman PA (2010) AMBER 11; University of California San Francisco
77. Hornak V, Abel R, Okur A, Strockbine B, Roitberg A, Simmerling C (2006) Comparison of multiple amber force fields and development of improved protein backbone parameters. Proteins 65:712–725
78. Onufriev A, Bashford D, Case DA (2004) Exploring protein native states and large-scale conformational changes with a modified generalized born model. Proteins 55:383–394
79. Daura X, Gademann K, Jaun B, Seebach D, van Gunsteren WF, Mark AE (1999) Peptide folding: when simulation meets experiment. Angew Chem Int Ed 38:236–240
80. Wang JM, Wang W, Kollman PA, Case DA (2006) Automatic atom type and bond type perception in molecular mechanical calculations. J Mol Graph Model 25:247–260
81. Wang JM, Wolf RM, Caldwell JW, Kollman PA, Case DA (2004) Development and testing of a general amber force field. J Comput Chem 25:1157–1174
82. Jorgensen WL, Chandrasekhar J, Madura JD, Impey RW, Klein ML (1983) Comparison of simple potential functions for simulating liquid water. J Chem Phys 79:926–935
83. Darden T, York D, Pedersen L (1993) Particle mesh Ewald - an NLog(N) method for Ewald sums in large systems. J Chem Phys 98:10089–10092
84. Hess B, Bekker H, Berendsen HJC, Fraaije JGEM (1997) LINCS: a linear constraint solver for molecular simulations. J Comput Chem 18:1463–1472
85. Khandogin J, Brooks CL (2007) Linking folding with aggregation in Alzheimer's β-amyloid peptides. Proc Natl Acad Sci USA 104:16880–16885
86. Yan YL, Wang CY (2006) Aβ 42 is more rigid than Aβ 40 at the C terminus: implications for Aβ aggregation and toxicity. J Mol Biol 364:853–862
87. Hou LM, Shao HY, Zhang YB, Li H, Menon NK, Neuhaus EB, Brewer JM, Byeon IJL, Ray DG, Vitek MP, Iwashita T, Makula RA, Przybyla AB, Zagorski MG (2004) Solution NMR studies of the Aβ(1–40) and Aβ(1–42) peptides establish that the met35

oxidation state affects the mechanism of amyloid formation. J Am Chem Soc 126:1992–2005
88. Liu RT, McAllister C, Lyubchenko Y, Sierks MR (2004) Residues 17–20 and 30–35 of beta-amyloid play critical roles in aggregation. J Neurosci Res 75:162–171
89. Baumketner A, Shea JE (2007) The structure of the Alzheimer amyloid β 10–35 peptide probed through replica-exchange molecular dynamics simulations in explicit solvent. J Mol Biol 366:275–285
90. Riek R, Güntert P, Döbeli H, Wipf B, Wüthrich K (2001) NMR studies in aqueous solution fail to identify significant conformational differences between the monomeric forms of two Alzheimer peptides with widely different plaque-competence Aβ(1–40)ox and Aβ(1–42)ox. Eur J Biochem 268:5930–5936
91. Yu L, Edalji R, Harlan JE, Holzman TF, Lopez AP, Labkovsky B, Hillen H, Barghorn S, Ebert U, Richardson PL, Miesbauer L, Solomon L, Bartley D, Walter K, Johnson RW, Hajduk PJ, Olejniczak ET (2009) Structural characterization of a soluble amyloid β-peptide oligomer. Biochemistry 48:1870–1877
92. Bitan G, Kirkitadze MD, Lomakin A, Vollers SS, Benedek GB, Teplow DB (2003) Amyloid β-protein (Aβ) assembly: Aβ40 and Aβ42 oligomerize through distinct pathways. Proc Natl Acad Sci USA 100:330–335
93. Schmidt M, Sachse C, Richter W, Xu C, Fandrich M, Grigorieff N (2009) Comparison of Alzheimer Aβ(1–40) and Aβ(1–42) amyloid fibrils reveals similar protofilament structures. Proc Natl Acad Sci USA 106:19813–19818
94. Sánchez L, Madurga S, Pukala T, Vilaseca M, López-Iglesias C, Robinson CV, Giralt E, Carulla N (2011) Aβ40 and Aβ42 amyloid fibrils exhibit distinct molecular recycling properties. J Am Chem Soc 133:6505–6508
95. Alonso H, Bliznyuk AA, Gready JE (2006) Combining docking and molecular dynamic simulations in drug design. Med Res Rev 26:531–568
96. Li J, Liu R, Lam KS, Jin LW, Duan Y (2011) Alzheimer's disease drug candidates stabilize A-β protein native structure by interacting with the hydrophobic core. Biophys J 100:1076–1082